Clays and Clay Minerals, Vol. 40, No. 1, 81–91, 1992.

FAR-INFRARED STUDY OF THE INTERLAYER TORSIONAL-VIBRATIONAL MODE OF MIXED-LAYER ILLITE/SMECTITES

PAUL A. SCHROEDER[1]

Department of Geology and Geophysics, Yale University, P.O. Box 6666
New Haven, Connecticut 06511

Abstract—Investigation of mixed-layer illite/smectites with far-infrared (FIR) spectroscopy indicates the presence of torsional mode absorption bands associated with interlayer fixed-K sites. By contrast, hydrated montmorillonitic interlayer cation sites are transparent in the far IR. The presence or absence of bands for interlayer cation sites appears to be related to both the magnitude and site of negative layer charge within the 2:1 layer structure. The bimodal nature of illite/smectite spectra leads to the suggestion that two different fixed-K environments occur within illite/smectite structures. These two environments are controlled by the composition of the octahedral sheet. The torsional modes at 112 and 89 cm^{-1} represent fixed-K sites influenced, respectively, by an Al-rich, high-charge dioctahedral layer and a heterogeneous Al-Fe-Mg-bearing, low-charge layer. A general trend of increasing absorption of the 112 cm^{-1} band, relative to the 89 cm^{-1} band, is observed in a typical diagenetic illite/smectite sequence of Miocene shales from the Gulf of Mexico sedimentary basin. The absorbance strength of both torsional bands is also seen to increase with increasing degree of illitization and the amount of fixed potassium in the illite/smectite. These observations are consistent with the concept of shales undergoing illitization during burial diagenesis by both the collapse of high-charge smectite layers to form illite layers (i.e., transformation) and the formation of new high-charge (−0.9) illite layers at the expense of smectite layers (i.e., dissolution/neoformation).

Key Words—Burial diagenesis, Far-infrared, Illite/smectite, Miocene shale, Terrebonne Parish, Louisiana, X-ray diffraction.

INTRODUCTION

The exact chemical structure of mixed-layer illite/smectites (I/S) has long been the subject of discussion because of the importance of their thermodynamic and kinetic properties in controlling common weathering and diagenetic reactions (Garrels, 1984). The analytical techniques of X-ray diffraction and major oxide analysis are the primary means used to elucidate I/S crystal chemistry (MacEwan and Ruiz-Amil, 1975; Hower *et al.*, 1976; Reynolds, 1980; Środoń *et.al.*, 1986; Eberl and Środoń, 1988). Ancillary techniques such as electron microscopy (Nadeau *et al.*, 1984a, 1984b, 1984c; Inoue *et al.*, 1987; Ahn and Buseck, 1990), IR spectroscopy (Juo and White, 1969; Farmer and Velde, 1973; Sayin and Reichenbach, 1978; Velde, 1983) and nuclear magnetic resonance spectroscopy (Kirkpatrick *et al.*, 1986; Weiss *et al.*, 1987; Altaner *et al.*, 1988; Woessner, 1989) have provided additional constraints on the crystallographic and chemical details of I/S. Theoretical electrostatic potential calculations have also improved our perception of 2:1 phyllosilicate structures (Giese, 1971; Bleam, 1990), and it appears that the ability to predict large clay mineral structures accurately via *ab initio* electron wavefunction calculations and molecular dynamics will emerge toward the end of this decade (Lasaga, 1990). Despite these vast strides in our understanding of the crystal and chemical state of I/S, there are still ambiguities regarding the nature of their structure (Altaner *et al.*, 1988). A large part of this ambiguity originates from the lack of self-consistency among the various analytical techniques. Therefore, any additional technique(s) that can independently corroborate the current models for I/S crystal chemistry would certainly be of benefit.

As suggested by Schroeder (1990), the nature of the interlayer torsional-vibrational mode of mica structures may help provide an additional constraint on the structure of layer charged 2:1 phyllosilicates. This vibrational mode is observed as a strong absorption band in the far-IR region, whose frequency is strongly correlated with the charge and mass of the interlayer cation and the composition of the octahedral layer (Fripiat, 1982; Grupta *et al.*, 1988; Laperche and Prost, 1989; this study). The interlayer torsional mode of micaceous 2:1 phyllosilicates is typically observed in the frequency range of 50–115 cm^{-1}. Translational interlayer modes are also indentified at slightly higher freqeuencies, in the 120–180 cm^{-1} range. However, in contrast to the torsional mode, these modes typically exhibit much lower absorbance values. With its relative ease of detection, the torsional mode offers a greater potential for application in multiphase natural systems and, therefore, is the focus of this study.

[1] Present address: Department of Geology, The University of Georgia, Athens, Georgia 30602.

The purpose of this study is to assess the relationship between the frequency and intensity of the interlayer torsional mode(s) and the crystal-chemical properties of mixed-layer I/S. The first objective of this study is to discriminate absorption bands of I/S that are associated with fixed cations from those potentially associated with exchangeable cations. The known dependency of frequency on both the exchangeable cation charge and mass (as seen in vermiculite) and on the octahedral composition (as seen in K micas) provides the basis for this examination. A second aspect of this work addresses the implications of band frequency and intensity for characterization of the I/S structure. As part of this second goal, aim is taken at the investigation of the FIR spectra of Miocene shales sampled from the Gulf of Mexico sedimentary basin.

MATERIALS AND METHODS

Samples and sample preparation

Mineral specimens used in this study were chosen in order to examine a range of mixed-layer states and the effect of the site of layer charge. These minerals include: The Clay Minerals Society Source Clay Repository reference materials IMt-1 (illite; Silver Hill, Montana), ISMt-1 (K-bentonite; Mancos shale), SCa-1 (Ca-montmorillonite; Otay, California), SWy-1 (Na-montmorillonite; Crook Co., Wyoming), VTx-1 (vermiculite; Llano, Texas) and a mixed-layer I/S (Cameron, Arizona; Yale Peabody Museum #002M-DS1). A sequence of natural mixed-layer I/S, from a well located in Terrebonne Parish, Louisiana, was also studied as representative of samples from a burial diagenetic environment. The natural I/S samples used were drill cuttings from Miocene shale intervals, collected over the depth range of 1220–5764 m (Table 1). Shale chips were hand-picked to avoid potential drilling mud contamination.

All samples were gently disaggregated and sieved to remove the >45.0-μm fraction. Several chemical treatments were then applied to the samples in order to purify them before analysis. Labile organics were removed using H_2O_2. Iron oxide and oxyhydroxide coatings were removed using a pH 7.6 buffered citrate-dithionate-bicarbonate solution (Ruttenberg, 1990), and carbonates were removed using pH 4 buffered sodium acetate-acetic acid (Moore and Reynolds, 1989). All samples were subsequently sized to the <2.0-μm (equivalent spherical diameter) fraction by centrifugation (Hathaway, 1956). In order to keep grain size effects comparable, the reference materials were sized to the <1.0-μm fraction. The shale samples were further sized to the <0.2-μm fraction to concentrate the diagenetic clay.

Saturation of the exchangeable cation sites in the various clays was performed through standard treatment with 1 M chloride solutions for univalent cations and 0.1 M solutions for divalent cations. The effectiveness of the saturation treatment was checked with a Scintag Pad-V X-ray diffractometer by measurement of the basal (001) reflections (MacEwan and Wilson, 1980) using slurry-sedimented mounts on quartz plates at the ambient relative humidity of the laboratory (~50%). Cation-exchanged vermiculites were examined by X-ray diffraction (XRD) to demonstrate the effect of different ionic radii on the d(001) distance. Sedimented mounts were heated at 100°C for 24 hours to remove the hydration sphere. To minimize rehydration effects, samples were scanned in the diffractometer within 30 seconds from removal from the oven.

Analytical techniques

The inability to separate the discrete kaolinite and illite from the diagenetic I/S clay fraction in the shale cuttings necessitated quantitative clay mineralogy of the <0.2-μm fraction. The procedure involved the use of model XRD patterns calculated by the program NEWMOD (Reynolds, 1985). The quantitation was obtained using the following procedure: 1) XRD data were collected from Ca^{2+}- and ethylene glycol-saturated mounts, sedimented from slurries to infinite thickness; 2) the percentage of illite in the I/S was determined using the differential measurement of the reflections in the 43°–48°2θ CuKα region (Środoń, 1980). Peak positions of the mixed-layer I/S (005/008) and (005/009) and the illite (005) reflections were determined from fitted Gaussian curves using a least-squares routine supplied by Scintag; 3) using a quartz standard, appropriate instrument-sensitive NEWMOD parameters were tuned to best-fit the Scintag diffractometer optics; 4) the remaining tunable sample-sensitive NEWMOD parameters were further determined by using independent compositional data and trial-and-error to best-fit model output with observed diffraction data. Parameters used in the final calculations were: the range of number of unit cells stacked in a coherent scattering array, N = 10–18 for the kaolinite; N = 7–14, K^+ = 0.75, Fe^{2+} = 0.2 for the illite; and a mean defect-free distance of 3 unit cells over a coherent scattering domain of 6 unit cells (K^+ = 0.75, Fe^{3+}_{illite} = 0.2 and $Fe^{3+}_{smectite}$ = 0.4 for the I/S); 5) reference intensity ratios (RIR) (Chung, 1975) were then calculated for each model using the 2θ range 22°–35°, at 0.1° increments, using kaolinite as the reference standard; 6) a least-squares minimization technique was used to fit model diffraction data with observed diffraction data (Smith *et al.*, 1987); 7) appropriate RIRs were applied to obtain the relative abundance of each clay mineral; and 8) as a check, a final model diffraction data set was computed with the derived weight fractions. Observed and model diffraction data were then visually compared to verify a reasonable degree of fit (see Figure 1 for examples of results). It is important to realize that the diffraction patterns of most natural samples are best modeled as a population with a range of particle sizes, chemistries, defects and Reichweite properties. However, for ease of characterization and consistency in reporting, average values for the fraction of illite in the mixed-layer I/S and Reichweite (R) were employed.

FIR absorption spectra were collected on a Nicolet SX-60 FTIR spectrometer using a 25-μm thick Mylar beam splitter, Globar source, DTGS detector and water/CO_2-purged atmosphere. Spectral resolution was set at 4 cm^{-1} with a time-averaged signal collected over 200 scans. Peak positions were reproducibly measured ±0.5 cm^{-1}. Spectral data in the 120–140 cm^{-1} region are either interpolated or not reported for the following reasons. Firstly, the 25-μm beam splitter has very poor efficiency in this region. Secondly, the acquisition of a sample IR spectrum relies on the ratio of the sample signal to a blank instrument signal, in order to remove non-linear instrumental effects. Ideally, the instrument mirror and sample chambers are purged of gaseous CO_2 and H_2O, because these molecules absorb IR radiation. An ineffective purge leaves residual gases in the chambers. As a consequence, a significant overprint from the rotational bands of water can be imparted on the spectrum (Hofmeister *et al.*, 1989). The combined effects of poor beam splitter efficiency and difficulty in duplicating purge conditions result in spurious signals for the 120–140 cm^{-1} region.

Samples were sedimented either on an IR-grade silicon wafer (Schroeder, 1989) or made to form a self-supporting film. Sample densities were determined by independent weight measurements (using a microbalance) and area measurements (using a microscope with an attached image analyzer). Rigorous quantitative assessment of the IR data could not be

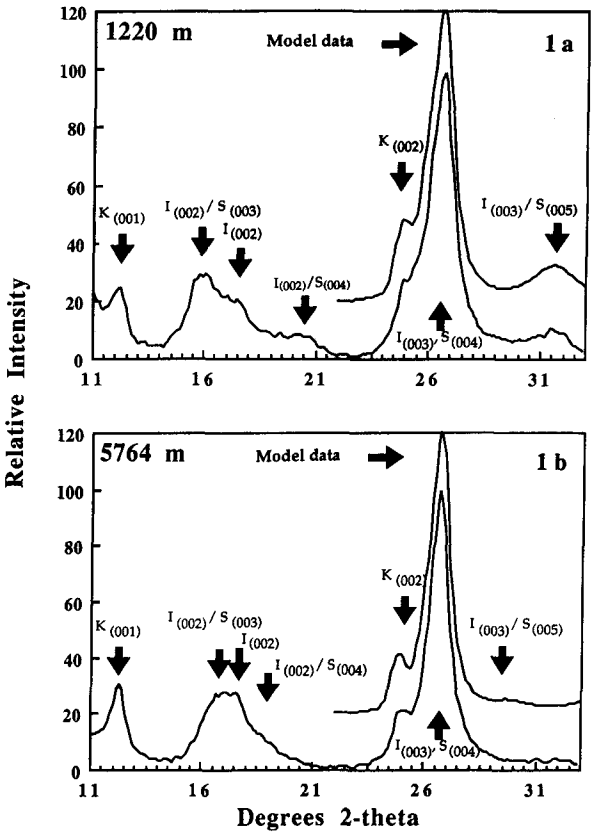

Figure 1. Observed and model X-ray diffractograms for the <2-μm fraction from depth intervals (a) 1220 m and (b) 5764 m. The observed data are shown in the angular range of 11° to 33°2θ. Each peak has its respective (00l) reflection labeled. Plotted above the observed data, in the angular range of 22° to 33°2θ, are the quantitative modelling results, derived using calculated data and a least-squares fitting method (see text).

addressed in this study because absolute calibration studies were not performed and because of instrument stability limitations. A simplified assessment is still possible, however, through application of the Bouger-Beer law:

$$-\log\left(\frac{I}{I_0}\right) = A = kcc'l, \quad (1)$$

which states that absorbance (A) is a product of a proportionality constant (k) related to the absorptive power of the sample; the concentration of a constituent in a phase (c); the concentration of the phase in a mixture (c'); and the path length of the IR beam in the sample (l) (Smith, 1965). I_0 and I are the intensities of incident and transmitted IR radiation, respectively.

Major oxide analyses were performed with a JEOL TXA-8600 electron microprobe using standard techniques (Gulson and Lovering, 1968). Independently calibrated standards and sample unknowns were fused with a pre-ignited lithium tetraborate-lithium carbonate-lanthanum oxide flux in a sample-to-flux ratio of 1:10 (Wittkop and O'Day, 1973). Analyses were carried out using a voltage of 15 KeV, a Faraday cup current of 20 nA and a beam diameter of 50 μm. Standard deviation in the counting measurements averaged about ±3%

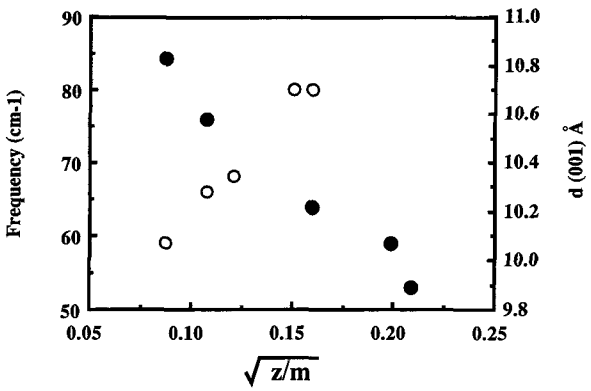

Figure 2. Linear dependence of torsional mode vibrational frequency (open circles) and d(001) of heated samples (solid circles) on the square root of the interlayer cation formal charge (z) and atomic mass (m) in Llano vermiculite (VTx-1).

of the measured value for each element, except Na_2O, which averaged about ±10%. Total iron is reported as Fe_2O_3.

RESULTS

The discrimination of torsional bands associated with fixed-K sites from those associated with exchangeable interlayer cation sites is of primary concern. For a vermiculite, where the compensating interlayer cations can be homoionically exchanged, previous workers have shown the nature of the cation influences both torsional band behavior and lattice dimensions (Fripiat, 1982; Laperche, 1991). To illustrate this effect, the torsional mode band frequencies of cation-exchanged, hydrated Llano vermiculite and the d(001) of dehydrated Llano vermiculite were measured with IR and XRD, respectively. Figure 2 shows the clear dependency of both band frequency and d(001) on the formal charge (z) and atomic mass (m) of the interlayer cation. The torsional band frequencies observed here are similar to those observed by Fripiat (1982) and Laperche (1991).

Figure 3 shows the FIR spectrum for air-dried, hydrated Cs-saturated illite, revealing two strong absorption bands at frequencies 107 and 93 cm^{-1}. Based upon previous studies of K-micas, these bands are assigned to the torsional mode of the interlayer cations (Laperche and Prost, 1991). Notably, the band frequencies in this region do not change upon saturation with the cations NH_4^+, Na^+, K^+, Ca^{2+}, Rb^+, Sr^{2+} or Ba^{2+} (all spectra are experimentally identical and it is for this reason that only the one Cs-saturated spectrum is shown). Figure 3 also shows spectra for Cs-saturated K-bentonite and Arizona-I/S in the air-dried, hydrated state. Two absorption bands, slightly broader than those of the illite, appear at approximately 112 and 89 cm^{-1}. Like the illite, the torsional bands of the I/S do not shift when saturated with different cations. The XRD patterns of the K-bentonite and Arizona-I/S were simulated with NEWMOD using sample-sensitive model

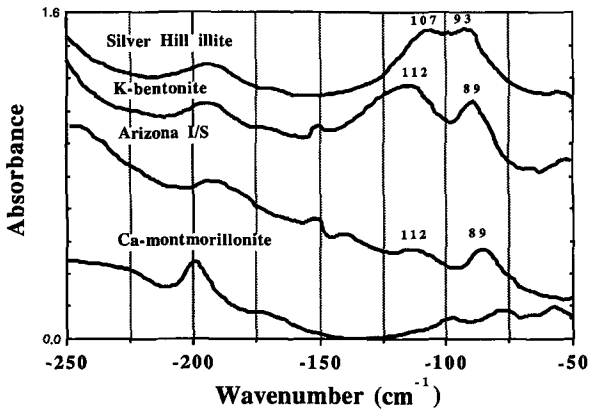

Figure 3. Far-infrared spectra of illite/smectite reference materials. The average number of illite (10 Å) layers (I) and ordering of the structures (R) are, respectively: Silver Hill illite (IMt-1), I = 0.95, R = 3; Mancos shale K-bentonite (ISMt-1), I = 0.65, R = 1; Arizona I/S (2M-DS1), I = 0.50, R = 0; and SCa-1, I = 0.02, R = 0. Data between 120 and 140 cm^{-1} have been interpolated, because of poor beam-splitter efficiency (see text).

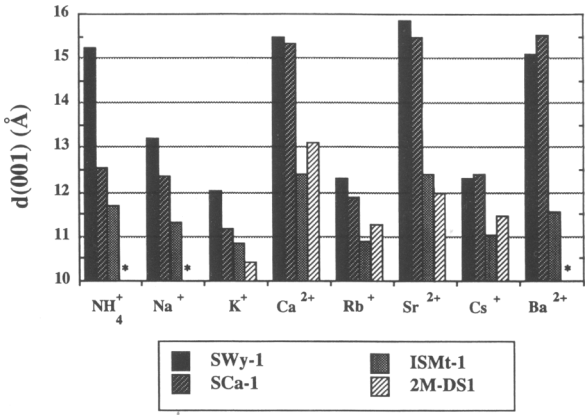

Figure 4. D-spacing of basal (001) reflection for smectite and illite/smectite reference materials upon cation saturation treatment. Distances are for samples in the hydrated state at a relative humidity of 50% ± 15%. *Not determined.

parameters of DIMICA = 0.65, DISMECTITE-2GLY = 0.35, R = 1; and DIMICA = 0.50, DISMECTITE-2GLY = 0.50 and R = 0, respectively. In order to ascertain whether the low-frequency band below 100 cm^{-1}, as seen in these mixed-layer illitic clays, represents an exchangeable cation site with no functional charge/mass dependency or represents a fixed-K site, cation-exchanged montmorillonites were also examined.

The FIR spectrum for air-dried, hydrated Cs-saturated Ca-montmorillonite shows no significant absorption bands in the range 50–120 cm^{-1} (Figure 3). With the exception of the weak absorption band at 97 cm^{-1}, the small spectral features in the low-frequency region are not reproducible. Although not shown, Na-montmorillonite also does not exhibit obvious, reproducible absorption bands in the low-frequency region. Both montmorillonites, regardless of cation saturation, have no interlayer cation charge/mass-dependent bands, even though XRD data indicated that effective cation saturations were achieved (Figure 4). The weak band at 97 cm^{-1} observed in SCa-1 shows no frequency dependence upon cation saturation state. These FIR observations of montmorillonite are consistent with those of Velde and Couty (1985).

Table 1. Chemical microprobe analysis of reference clays and <0.2-μm fraction of Miocene shale cuttings, Terrebonne Parish, Louisiana.

Sample[1]	IMt-1	ISMt-1	2M-DS1	1220 m	1577 m	2568 m	2779 m	3172 m
SiO_2	55.10	50.72	49.38	50.85	50.79	50.09	50.42	50.64
TiO_2	0.63	0.31	0.80	1.03	1.25	1.33	1.04	1.10
Al_2O_3	22.00	28.58	22.39	21.22	21.73	23.81	22.78	22.53
Fe_2O_3	6.78	0.98	9.04	7.47	7.55	6.73	5.67	6.63
MgO	2.80	2.45	2.69	3.31	3.43	2.98	3.29	3.09
CaO	<0.01	<0.01	<0.01	<0.01	<0.01	<0.01	<0.01	<0.01
Na_2O	0.08	1.03	1.26	1.05	0.89	0.79	0.91	0.93
K_2O	8.04	5.46	3.36	2.55	2.72	3.06	2.68	2.87

Sample	3483 m	3758 m	4178 m	4361 m	4673 m	5093 m	5368 m	5764 m
SiO_2	50.54	49.44	50.19	48.71	48.25	49.20	46.86	47.91
TiO_2	0.81	0.82	0.90	0.95	1.34	1.08	0.75	1.39
Al_2O_3	22.45	22.59	22.74	23.21	23.34	24.55	21.66	22.79
Fe_2O_3	6.84	6.40	6.06	6.59	6.27	6.11	6.15	5.50
MgO	3.11	2.89	3.10	2.87	2.79	3.05	2.55	2.78
CaO	<0.01	<0.01	<0.01	<0.01	<0.01	<0.01	<0.01	<0.01
Na_2O	0.95	1.06	1.17	1.07	1.22	0.62	1.99	1.35
K_2O	3.21	3.33	3.33	3.41	3.58	3.96	3.46	3.72

[1] IMt-1 = Cambrian shale, Silver Hill, Montana; ISMt-1 = Ordovician Mancos shale; 2M-DS1 = shale, Cameron, Arizona (Yale Peabody Museum #002M-DS1); shale identifications are given by sample depth, in meters.

Major oxide analyses for some of the reference materials and the Miocene samples studied are presented in Table 1.

Table 2 contains the normalized, quantitative XRD analysis of the <0.2-μm fraction of the Miocene shale samples. Accuracies of the reported weight fractions amount to ±20% of the values listed. Relative precision of the values is ±5%. Obvious features seen in Table 2 are an increase in the amount of illite with depth and an increase in the percentage of illite layers in the I/S. Calculation of the total number of illite layers (I_T = illite + % illite × I/S) shows an increase with increasing depth of burial.

The FIR spectra of the <0.2-μm fraction, Cs-saturated Miocene shales are presented in Figure 5. The band(s) around 196 cm^{-1}, as suggested by Velde and Couty (1985), can be assigned to a vibrational mode involving octahedral aluminum motions relative to the Si Al–O lattice of the tetrahedral sheet. This band can therefore be attributed to all the phyllosilicate phases present, including kaolinite, illite and I/S. The lower frequency torsional modes, like those in the reference I/S, are characterized by two broad bands with maximum absorbance occurring at 112 and 89 cm^{-1}. Like the reference I/S, the shale separates are also insensitive to hydrated exchangeable cation saturation states.

Several observations can be made regarding the torsional bands in this I/S series. Firstly, the frequencies of the bands do not shift with either the depth of sampling, fraction of illite layers in the I/S, or K_2O content of the I/S. Secondly, the ratio of the 112 cm^{-1} to 89 cm^{-1} band intensities increases with depth. This second relationship may be subtly apparent. However, one must recall that there are admixtures of illite and kaolinite in the specimens. Intensities of the bands at 112 cm^{-1} and 89 cm^{-1} were measured by estimating a linear background using adjacent absorption minima, and drawing a perpendicular line to the peak maxima at 112 and 89 cm^{-1}. Figure 6 is a plot of the sample depth versus the ratios of the 112 to 89 cm^{-1} band intensities. A final observation includes the general trend of increasing total absorbance of the 112 and 89 cm^{-1} bands with increasing K_2O content of the I/S (Figure 7). The K_2O content of the I/S was derived using Eq. 2,

$$K_2O_{I/S} = \frac{K_2O_{TOT} - W_I K_2O_I}{W_{I/S}}, \qquad (2)$$

where W is the weight-fraction of illite (I) and I/S (Table 2), and K_2O is the oxide weight-fraction (Table 1 and assumed K_2O_I = 0.09).

Table 2. Depths, clay mineral weight-fractions, percent illite layers in I/S, and the number of illite layers for the <0.2-μm fraction of Miocene shale cuttings, Terrebonne Parish, Louisiana.

Depth (m)	Kaolinite	Illite	I/S	% Illite in I/S	Illite[1] layers
1220	0.08	0.12	0.80	40	0.44
1577	0.11	0.08	0.80	42	0.42
2568	0.15	0.12	0.72	44	0.44
2779	0.09	0.13	0.77	43	0.46
3172	0.06	0.19	0.74	47	0.54
3483	0.07	0.16	0.76	51	0.55
3758	0.07	0.18	0.74	54	0.58
4178	0.10	0.15	0.75	56	0.57
4361	0.10	0.15	0.75	59	0.59
4673	0.12	0.21	0.66	60	0.61
5093	0.09	0.22	0.67	63	0.64
5368	0.08	0.19	0.69	65	0.64
5764	0.08	0.19	0.71	68	0.67

[1] The total fraction of illite type layers = {weight-fraction of illite + [weight-fraction of I/S × (percent illite in illite/smectite ÷ 100)]}.

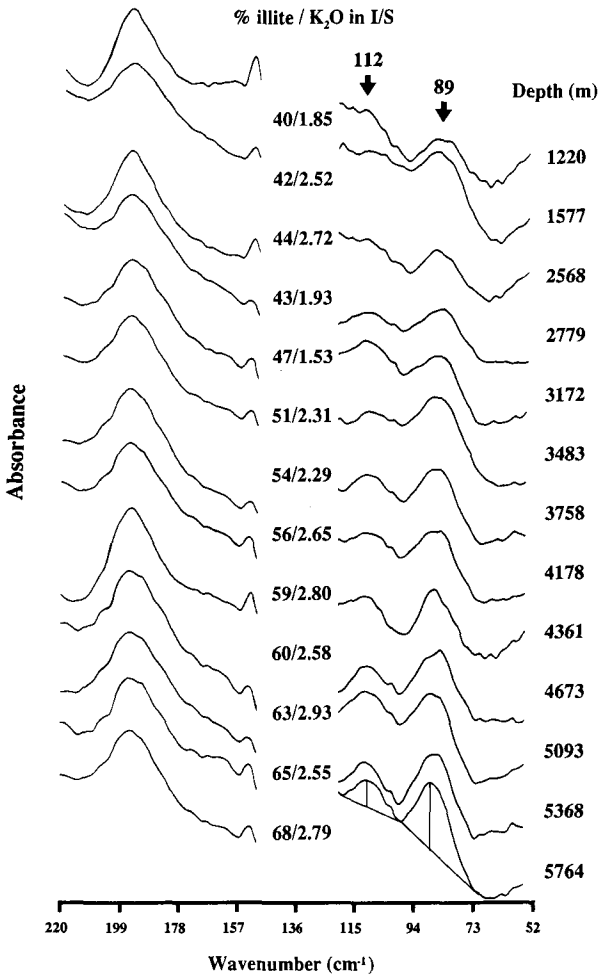

Figure 5. Far-infrared spectra of <0.02-μm fraction of Miocene shales from the Gulf of Mexico sedimentary basin. Sample depths are given to the right of each spectrum. The average percent of illite layers in the illite/smectite (I/S) and the K_2O content of the I/S are presented in the vacant data region of the spectra. Data in the 120 and 140 cm^{-1} region are not shown because of poor beam-splitter efficiency. The method of absorbance measurements at 112 cm^{-1} and 89 cm^{-1} is illustrated in the lowermost spectrum.

DISCUSSION

Identification and detection of fixed versus exchangeable cation sites

The presence of torsional bands in the spectra of vermiculite and beidellite (Fripiat, 1982) and the absence of torsional bands in the spectra of montmorillonites indicate that both the amount and the site of layer charge are important factors in detecting exchangeable cation sites with far-IR spectroscopy. In the case of vermiculite, the presence of a torsional mode absorption band indicates that most of the interlayer cations within the basal oxygen cavities occupy a unique equilibrium position. This may be attributed to both the modest amount of layer charge (−0.45 per half unit cell) and the location of charge from within the tetrahedral sheet. Stacking defects between layers and ordering of the layer structures may also be an important factor controlling the strength of the absorption band. For vermiculites, the location of layer charge in the tetrahedral sheet facilitates a relatively regular stacking order of the layers (de la Calle and Suquet, 1988). The presence of torsional mode absorption bands may coincide with the near-ideal layer shifts associated with the 1*M* polytype typical of vermiculites.

In a similar fashion to the vermiculite, the torsional band frequency of beidellite responds to the charge and mass of the exchangeable cation (Fripiat, 1982). The higher frequencies of the bands for the cations Cs, Ba and K in beidellite (85, 80 and 100 cm^{-1}) relative to vermiculite (59, 68 and 80 cm^{-1}) can be attributed to the dioctahedral nature of the octahedral sheet. The asymmetrical charge distribution in the dioctahedral structure influences the orientation of bound hydroxyl, thereby lowering repulsive proton-interlayer cation forces (Prost and Laperche, 1990). The origin of the beidellite layer charge, like vermiculite, is from within the tetrahedral sheet. However, in contrast to vermiculite the total net layer charge is smaller. No absorbance measurements were made on beidellite in this study, therefore no comparisons of absorption strength could be made. It would be informative to see if the smaller number of exchangeable sites and wider deviations from ideal stacking order in beidellite, relative to vermiculite, would lead to weaker torsional band absorbance values for samples with equivalent thickness.

The Na- and Ca-montmorillonites have average layer charges of −0.31 and −0.43 per half unit cell, respectively (van Olphen and Fripiat, 1979; Earley *et al.*, 1953). The absence of coherent absorption bands in both indicates that when the site of the layer charge is both small and within the octahedral sheet the forces between the interlayer cations and the basal and hydroxyl oxygens are too diffuse to establish a single equilibrium position. The d-spacings of the (001) reflections also indicate that the cations are hydrated (Figure 4). It is important to note that there are observable torsional modes in structures whose layer charge is primarily octahedral. This is the case for celadonites where the net layer charge is about −0.9.

From the above observations, there appears to be a threshold that involves both the *location* and *amount* of layer charge. The support for the threshold concept comes from the facts that: 1) bands are observed in 2:1 clays that have modest to high layer charge, originating from either the octahedral or tetrahedral sheet and in 2:1 clays that have low layer charge originating from the tetrahedral sheet, and 2) bands are not observed in 2:1 clays that have low charge originating from the octahedral sheet. This threshold may be raised by the processes of dehydration of the interlayer cation to collapse the structure into a more ordered state. Removal of the hydration sphere about the interlayer cation may improve stacking order and enhance the likelihood for coherent absorption. Unfortunately, instrumental limitations did not allow investigation of samples in the dehydrated state. Responses of FIR spectra to dehydration can only be speculated upon at this point, but appear to be fruitful ground for further experimentation.

The understanding of the response of the torsional mode to layer charge and compensating cations as learned from this study and others (Prost and Laperche, 1990; Schroeder, 1990; Laperche, 1991; Laperche and Prost, 1991) gives insight into the interpretation of the torsional bands observed in I/S. It appears reasonable to assign the bands observed in I/S to interlayer cations that are fixed by sheets whose layer charge is large (greater than −0.5?) and/or predominantly originates from the tetrahedral sheet. Insensitivity of the I/S spectra to hydrated cation saturation states indicates that the exchangeable montmorillonite sites are transparent to FIR detection.

Implications of band frequencies for I/S structure

If it is assumed that exchangeable cations in I/S are not responsible for interlayer torsional absorption bands, the torsional bands in the spectra can be ascribed to fixed K. In this way, their frequencies and bimodal nature offer specific information about I/S crystal chemistry. For a given fixed homoionic interlayer composition, the study of true micas (*sensu stricto,* Bailey, 1984) indicates that the frequency of the torsional mode is primarily controlled by the composition of the octahedral sheet. Based on this premise, it is possible to use the empirical relationship proposed by Schroeder (1990) for predicting vibrational frequency from octahedral sheet composition in order to assess the chemical nature of the sheets surrounding fixed-K sites. Equation 3 is a simplified version of that relationship, assuming that no F^- or Li^+ occupy the octahedral layer and that all the iron is Fe^{3+}. It has

been rearranged to yield the aluminum composition of the octahedral sheet, given the frequency of the K torsional mode (ν_i^K) in wavenumbers, and the structural cation site composition in mole numbers based on 11 oxygen equivalents per formula unit:

$$Al_{oct} = \frac{\nu_i^K - 79.6 - 1.92Mg_{oct} + 18.18Fe^{3+}_{oct}}{15.22}. \quad (3)$$

It is important to realize that the initial correlation of octahedral composition and frequency was made using true micas only. Realizing that illite layers in I/S have net charges lower than -1.0 and the octahedral sheets contain subordinate amounts of Fe^{2+}, Eq. 3 is intended only to serve as a relative measure of octahedral sheet composition.

The oxide data from Table 1 have been recast into average structural formulae with 11 oxygen equivalents using the program CLAYFORM (Bodine, 1987):

IMt-1 (illite),
$K_{0.68}Na_{0.01}(Al_{1.34}Ti_{0.03}Fe^{3+}_{0.34}Mg_{0.28})(Si_{3.63}Al_{0.37})O_{10}(OH)_2$,

ISMt-1 (K-bentonite–I/S, I = 0.65, R ≈ 1),
$K_{0.47}Na_{0.14}(Al_{1.74}Fe^{3+}_{0.50}Mg_{0.29})(Si_{3.46}Al_{0.55})O_{10}(OH)_2$,

2M-DS1 (Arizona I/S, I = 0.50, R = 0),
$K_{0.30}Na_{0.16}(Al_{1.30}Fe^{3+}_{0.48}Mg_{0.28})(Si_{3.46}Al_{0.54})O_{10}(OH)_2$.

For the illite, K-bentonite and Arizona I/S the *average* aluminum octahedral contents are $Al_{oct} = 1.34$, $Al_{oct} = 1.74$, and $Al_{oct} = 1.30$, respectively. The occurrences of bands at 107 and 93 cm^{-1} in the illite and at 112 and 89 cm^{-1} in the I/S suggest that they possess two different fixed-K sites resulting from the influence of two distinct octahedral sheet compositions. The high frequency band at 107 cm^{-1} for the illite and 112 cm^{-1} for the I/S is similar to that of muscovite (108 cm^{-1}), implying an interlayer site whose structure is controlled by an Al-rich, muscovite-like dioctahedral sheet. If it is assumed that Fe^{3+} and Mg^{2+} are absent from this type of octahedral sheet, then Eq. 3 predicts octahedral sheet compositions of $Al_{oct} = 1.80$, $Al_{oct} = 2.13$, and $Al_{oct} = 2.13$, respectively. These octahedral molar values more closely resemble the values of muscovite than the values derived from the average formulae.

Fe^{3+} and Mg^{2+} in the octahedral sheet both have a frequency-lowering effect (Prost and Laperche, 1990; Schroeder, 1990). The low frequency band at 93 cm^{-1} for the illite and 89 cm^{-1} for the I/S likely reflects interlayer sites whose structures are dominated by larger, heterogeneous sheets (i.e., containing both di- and trivalent cations). If all the Fe^{3+} and Mg^{2+} are in the octahedral sheet, then Eq. 3 estimates octahedral sheet contents of $Al_{oct} = 1.26$, $Al_{oct} = 1.18$, and $Al_{oct} = 1.16$ for illite, K-bentonite and Arizona I/S, respectively. This layer type is hereafter referred to as the Al-Fe-Mg-bearing layer.

The bimodal nature of the torsional bands and the octahedral compositions predicted from Eq. 3 suggest that I/S is composed of not only a smectitic layer, but also two distinct fixed-K layer types within the mixed-layer structure, whose environments are controlled by contrasting octahedral sheet compositions. The higher frequency of the Al-rich dioctahedral layer band in the K-bentonite (112 cm^{-1}) relative to the illite (107 cm^{-1}), and the lower frequency of the Al-Fe-Mg-bearing layer band in the K-bentonite (89 cm^{-1}) relative to illite (93 cm^{-1}), can be attributed to the effects of octahedral cation charge distribution on the hydroxyl orientation, and possibly greater stacking disorder or number of lateral dislocations in the *ab*-plane of the K-bentonite structure.

The concept of compositionally different illite layer types was inferred as early as 1966 by Hower and Mowatt, who were seeking to explain why chemical analyses of illite yielded structural formulae with lower charges than true micas. Hower and Mowatt (1966) suggested that different layer types may be contained within different particle size populations, however their study saw no systematic differences in the chemistry of fractionated size ranges. The accepted value of -0.75 fixed-K layers per $O_{10}(OH)_2$ for end-member illite is an average value based upon an ideal single phase structural formula. Evidence presented by Środoń *et al.* (1986), based upon the analysis of fixed interlayer cation content and percent expandable layers over the entire I/S range, supports the notion of I/S being comprised of compositionally different illite layers. Their data indicate two types of fixed cation sites are present, one with layer charges in the region of -0.55 per $O_{10}(OH)_2$ (for randomly interstratified, R ≈ 0), and the other in the region of -1.0 per $O_{10}(OH)_2$ (for ordered, R > 0). They further suggest that illitic portions of diagenetic I/S transform through a process of K^+ fixation that involves both the collapse of preexisting smectitic layers into low-charge (-0.55) illitic layers and the crystal growth of new high-charge (-1.0) illitic layers.

Eberl and Środoń (1988) and Środoń *et al.* (1990) have subsequently reinterpreted the relationship between fixed interlayer cation content and expandability of I/S. They now attribute the trend to an artifact related to the measurement of expandability using the XRD method. The presence of non-swelling basal surfaces that form the ends of small (i.e., fundamental) illite particles creates additional coherent X-ray scattering domains that result in estimates of fewer expandable layers. This interpretation nicely reconciles the discrepancy between measurements of expandability made by the XRD method and those made by counting of layer types using the TEM method. Eberl and Środoń (1988) support their notion for the pres-

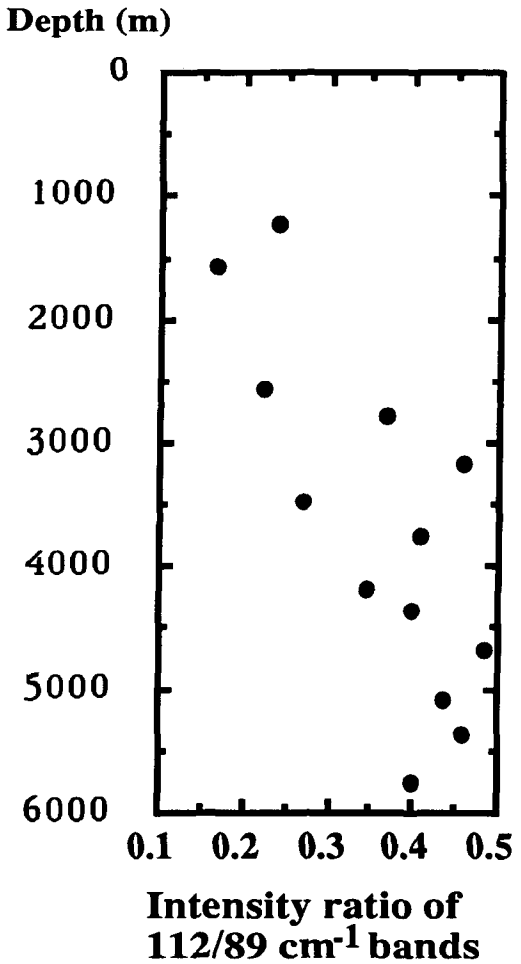

Figure 6. Ratio of the absorbance band intensities measured at 112 cm^{-1} and 89 cm^{-1} versus depth of sample for the Miocene shales.

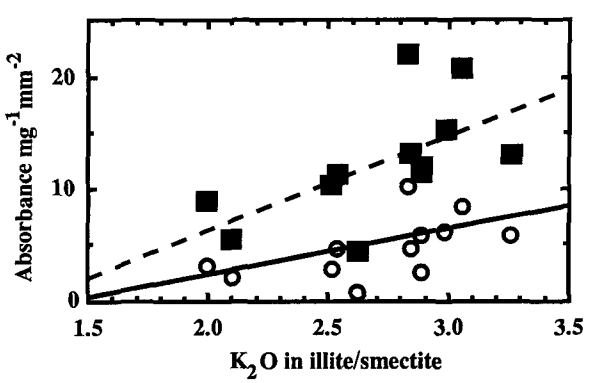

Figure 7. Absorbance values adjusted by independently-measured sample thickness versus the K_2O content of the illite/smectites in the Miocene shales. Open circles are values for the 112 cm^{-1} band. Closed squares are values for the 89 cm^{-1} band. The solid and dashed lines are visual aids, fitted to the circles and squares respectively, to show the generally positive trends.

ence of fundamental particles by citing Huff *et al.* (1988), who provide XRD and selected-area electron diffraction evidence for illite layer types existing in segregated illite and I/S domains. These more recent arguments properly bring to light the nature of illite particle surfaces, however there still remains the possibility for high- and low-charged illite layer types to exist.

The FIR evidence for an Al-rich, dioctahedral layer type and an Al-Fe-Mg-bearing layer type structure within I/S may be compatible with the low-K and high-K illite layer types proposed by Środoń *et al.* (1986). Unfortunately, the chemical and IR evidence offers no information about the ordering of these layer types. Octahedral sheet thicknesses for muscovite and phlogopite average about 2.09 Å and 2.15 Å, respectively (see Tables 1 and 2, in Bailey, 1984). One would have to resolve octahedral structures in illitic clays with systematic dimensional differences on the order of 0.06 Å in order to validate the concept of two illitic layer types. Therefore, TEM imaging evidence in recent papers does not necessarily directly support or refute the suggestion that compositionally different illite (10 Å) layers can exist.

Torsional band characteristics in a burial diagenetic sequence

The FIR spectra for diagenetic I/S from the Miocene shales provide insight into diagenetic transformation mechanisms with evidence for the existence of two illite layer types; an Al-rich dioctahedral layer type and an Al-Fe-Mg-bearing layer type. The persistence of the low frequency band at 89 cm^{-1} throughout the diagenetic sequence supports the idea of preservation of early formed, low-charge (−0.5) illite layers, derived from the collapse of originally high-charged (−0.5) smectitic layers (Środoń *el al.*, 1986).

The ratio of the absorbance values for the 112 and 89 cm^{-1} bands of the same sample cancels the effect of variable path length between samples (Eq. 1). This ratio provides a measure of the relative concentration of the number of fixed cation sites that contribute to absorption. This ratio cannot be recalculated into the ratio of the absolute values of the concentration of fixed-K sites primarily because the absorption coefficients (k) for each band are not known. The trend of band ratios for the diagenetic I/S versus depth shown in Figure 6, therefore, shows only that with increasing depth the 112 cm^{-1} band becomes stronger in relation to the 89 cm^{-1} band.

The relative band intensities, illustrated in Figure 7, provide more information. They show a general trend of increasing normalized absorbance with increasing K_2O in the I/S portion of the shale fine fraction for both the 89 cm^{-1} and 112 cm^{-1} bands. Several factors may account for these results. The magnitude and site of layer charge, as well as stacking disorder, are likely to influence absorption intensity. The absorbance in-

crease in the 89 cm^{-1} band with increased illitization could be attributed to either a greater number of similar equilibrium positions brought on by more ideal stacking order or the formation of new fixed-K sites associated with the Al-Fe-Mg-bearing layers. The increase in absorbance of the 112 cm^{-1} band with the K_2O content of the I/S can be more likely attributed to the increase in the number of Al-rich dioctahedral layers (i.e., crystal growth). Given the quality of the data in this study, it is not possible to discriminate between the above factors. More rigorous quantitative IR studies will be required to elucidate the relationships between K_2O content, stacking order (i.e., polytypism and defects) and absorption strength.

Recent high-resolution TEM study of I/S by Ahn and Buseck (1990) suggests the presence of structural heterogeneities. Although interlayer spacings of illite and collapsed smectite cannot be distinguished unambiguously by TEM, evidence for different stacking orders is suggested. R1 I/S samples are dominated by 1*Md* stacking disorder, although local regions of 1*M* ordering are observed.

The concept of two illite layer types may also be supported by the hydrothermal I/S transformation studies of Whitney and Northrop (1988). Based on closed system reactions, the oxygen-isotope resetting during illitization suggests a reaction that proceeds via two different reaction mechanisms. The two illite layer types recognized in this study may be compatible with those formed by layer collapse (partial $\delta^{18}O$ resetting) and those formed by crystal growth (complete $\delta^{18}O$ resetting).

CONCLUSIONS

Investigation of the far-infrared spectra of mixed-layer I/S suggests that the strength of absorbance is controlled by the magnitude and site of negative layer charge from within the 2:1 structure. Lattice defects and departure from ideal polytype stacking sequences may also be important factors affecting coherency of absorption. More rigorous study will be required to clarify the relationships between absorbance strength, concentration of fixed K, and polytypes. FIR spectra of mixed-layer I/S saturated with various cations indicate that the torsional motions of the basal oxygen ring about hydrated exchangeable cations are not coherent enough to allow for a strong observable band in the montmorillonite structure. This transparency to detection leads to the suggestion that the bimodal nature of illite/smectite FIR spectra results from the presence of two fixed-K environments in the illitic structure. These high- and low-frequency torsional bands can be assigned to two types of fixed-K sites influenced, respectively, by an Al-rich, high-charge dioctahedral layer and an Al-Fe-Mg-bearing, low-charge layer.

A general trend of increasing Al-rich type layers relative to Al-Fe-Mg-bearing type layers is observed in a typical burial diagenetic sequence from the Gulf of Mexico sedimentary basin. The increase in absorbance of both torsional bands with increase in degree of illitization and fixed-K content is consistent with the concept of formation of new Al-rich illite layers at the expense of smectite layers. The persistence of an Al-Fe-Mg-bearing illite-type layer (evidenced by FIR) is compatible with previous chemical studies that suggest the I/S formed by burial diagenesis is comprised of both low-charge (−0.5) illite layers formed from the collapse of smectite layers and high-charge (−1.0) illite layers formed by precipitation from solution (Środoń *et al.*, 1986).

The advent of Fourier transform IR spectrometers dedicated to the far-IR region should enable more precise and controlled conditions than those available for this study. The results presented here should encourage exploration of the relationships between low frequency vibrational modes and crystal-chemical properties of mixed-layer I/S such as hydration state, stacking order, polytypism, and crystallite size. This improved understanding now provides a basis for assessing the self-consistency of chemical and structural models for I/S and for minimizing ambiguities that arise from characterization via multiple analytical techniques.

ACKNOWLEDGMENTS

Financial support was provided by an unrestricted grant-in-aid from Texaco Exploration and Production Technology Division, Houston, Texas, and GSA Research Grant No. 3870–87. IR spectrometer time was made available through Mike Herron and Mike Supp at the Schlumberger-Doll Research Laboratory in Ridgefield, Connecticut. Samples were kindly provided by Ellen Faller at the Yale Peabody Museum and Andy Thomas at Texaco. The author benefited from discussions with Bob Berner, J. J. Fripiat, Jim Howard, Ellery Ingall and Bob Reynolds. The editorial assistance of Tony Lasaga, Jan Środoń and an anonymous reviewer are also greatly appreciated.

REFERENCES

Ahn, J. H. and Buseck, P. R. (1990) Layer-stacking sequences and structural disorder in mixed-layer illite/smectite: Image simulations and HRTEM imaging: *Amer. Mineral.* **75,** 267–275.

Altaner, S. P., Weiss, C. A., and Kirkpatrick, R. J. (1988) Evidence from ^{29}Si NMR for the structure of mixed-layer illite/smectite clay minerals: *Nature* **331,** 699–702.

Bailey, S. W. (1984) Crystal chemistry of the true micas: in *Micas 13, Reviews in Mineralogy,* S. W. Bailey, ed., Mineral. Soc. Amer., Washington, D.C., 13–60.

Bleam, W. F. (1990) Electrostatic potential at the basal (001) surface of talc and pyrophyllite as related to tetrahedral sheet distorsions: *Clays & Clay Minerals* **38,** 522–526.

Bodine, M. W. (1987) CLAYFORM: A Fortran 77 computer program apportioning the constituents in the chemical analysis of a clay or other silicate mineral into a structural formula: *Computers and Geosciences* **13,** 77–88.

Chung, F. H. (1975) Quantitative interpretation of X-ray diffraction patterns of mixtures. III. Simultaneous determination of a set of reference intensities: *Jour. Appl. Cryst.* **8,** 17–19.

de la Calle, C. and Suquet, H. (1988) Vermiculite: in *Hydrous Phyllosilicates 19, Reviews in Mineralogy,* S. W. Bailey, ed., Mineral. Soc. Amer., Blacksburg, Virginia, 455–496.

Earley, J. W., Osthaus, B. B., and Milne, I. H. (1953) Purification and properties of montmorillonite: *Amer. Mineral.* **38,** 707–724.

Eberl, D. D. and Środoń, J. (1988) Ostwald ripening and interparticle diffraction effects for illite crystals: *Amer. Mineral.* **73,** 1335–1345.

Farmer, V. C. and Velde, B. (1973) Effects of structural order and disorder on the infrared spectra of brittle micas: *Mineral. Mag.* **39,** 282–288.

Fripiat, J. J. (1982) Application of far infrared spectroscopy to the study of clay minerals and zeolite: in *Advanced Techniques for Clay Mineral Analysis,* J. J. Fripiat, ed., Elsevier, New York, 191–210.

Garrels, R. M. (1984) Montmorillonite/illite stability diagrams: *Clays & Clay Minerals* **32,** 161–166.

Giese, R. F. (1971) Hydroxyl orientation in muscovite as indicated by electrostatic energy calculations: *Science* **172,** 263–264.

Grupta, H. C., Mahanti, S. D., and Solin, S. A. (1988) Torsional mode frequency and elastic anisotropy in alkali vermiculites: *Phys. Chem. Mineral.* **16,** 291–294.

Gulson, B. L. and Lovering, J. F. (1968) Rock analysis using electron probe: *Geochim. Cosmochim. Acta* **32,** 119–122.

Hathaway, J. C. (1956) Procedure for clay mineral analysis used in the sedimentary petrology laboratory of the U.S. Geological Survey: *Clay Miner. Bull.* **3,** 8–13.

Hofmeister, A. M., Xu, J., Mao, H. K., Bell, P. M., and Hoering, T. C. (1989) Thermodynamics of Fe-Mg olivines at mantle pressures: Mid and far-infrared spectroscopy at high pressure: *Amer. Mineral.* **74,** 281–306.

Hower, J., Elsinger, E. V., Hower, M. E., and Perry, E. A. (1976) Mechanism of burial metamorphism of argillaceous sediment: 1. Mineralogical and chemical evidence: *Geol. Soc. Amer. Bull.* **87,** 725–737.

Hower, J. and Mowatt, T. C. (1966) The mineralogy of illites and mixed-layer illite/montmorillonite: *Amer. Mineral.* **51,** 825–854.

Huff, H. D., Whitman, J. A., and Curtis, C. D. (1988) Investigation of a K-bentonite by X-ray powder diffraction and analytical transmission electron microscopy: *Clays & Clay Minerals* **36,** 83–93.

Inoue, A., Kohyama, N., Kitagawa, R., and Watanabe, T. (1987) Chemical and morphological evidence for the conversion of smectite to illite: *Clays & Clay Minerals* **35,** 111–120.

Juo, A. S. R. and White, J. L. (1969) Orientation of the dipole moments of hydroxyl groups in oxidized and unoxidized biotite: *Science* **165,** 804–805.

Kirkpatrick, R. J., Oestrike, R., Weiss, C. A. W., Jr., Smith, K. A., and Oldfield, E. (1986) High-resolution ^{27}Al and ^{29}Si NMR spectroscopy of glasses and crystals along the join $CaMgSi_2O_6$-$CaAl_2SiO_6$: *Amer. Mineral.* **71,** 705–711.

Laperche, V. (1991) Etude de l'etat et de la localisation des cations compensateurs dans les phyllosilicates: Par des methodes spectrometriques: Ph.D. thesis, Université de Paris, France.

Laperche, V. and Prost, R. (1989) Far infrared study of compensating cations in clays: *Abstracts with program,* A.I.P.E.A. 9th Intern. Clay Conf., Strasbourg, France, 224.

Laperche, V. and Prost, R. (1991) Assignment of the far-infrared absorption bands of K in micas: *Clays & Clay Minerals* **39,** 281–289.

Lasaga, A. C. (1990) Atomic treatment of mineral-water surface reactions: in *Mineral-water Interface Geochemistry 23, Reviews in Mineralogy,* Michael F. Hochella and A. F. White, eds., Mineral. Soc. Amer., Washington, D.C., 17–85.

MacEwan, D. M. C. and Ruiz-Amil, A. (1975) Interstratified Clay Minerals: in *Soil Components 2,* J. E. Gieseking, ed., Springer-Verlag, New York, 265–334.

MacEwan, D. M. C. and Wilson, M. J. (1980) Interlayer and intercalation complexes of clay minerals: in *Crystal Structures of Clay Minerals and Their X-ray Identification,* G. W. Brindley and G. Brown, eds., Mineral. Soc., London, 197–248.

Moore, D. E. and Reynolds, R. C. (1989) *X-ray Diffraction and the Identification and Analysis of Clay Minerals:* Oxford Univ. Press, New York.

Nadeau, P. H., Wilson, M. J., McHardy, W. J., and Tait, J. M. (1984a) Interstratified XRD characteristics of physical mixtures of elementary clay particles: *Clay Miner.* **19,** 67–76.

Nadeau, P. H., Wilson, M. J., McHardy, W. J., and Tait, J. M. (1984b) Interparticle diffraction: A new concept for interstratified clays: *Clay Miner.* **19,** 757–769.

Nadeau, P. H., Wilson, M. J., McHardy, W. J., and Tait, J. M. (1984c) Interstratified clays as fundamental particles: *Science* **225,** 923–925.

Prost, R. and Laperche, V. (1990) Far-infrared study of potassium in micas: *Clays & Clay Minerals* **38,** 351–355.

Reynolds, R. C. (1980) Interstratified clay minerals: in *Crystal Structures of Clay Minerals and Their X-ray Identification,* G. W. Brindley and G. Brown, eds., Mineral. Soc., London, 249–303.

Reynolds, R. C. (1985) *NEWMOD, a Computer Program for the Calculation of Basal Diffraction Intensities of Mixed-layered Clay Minerals:* R. C. Reynolds, 8 Brook Rd., Hanover, New Hampshire 03755.

Ruttenberg, K. C. (1990) Diagenesis and burial of phosphorus in marine sediments: Ph.D. thesis, Yale University, New Haven, Connecticut.

Sayin, M. and von Reichenbach, H. G. (1978) Infrared spectra of muscovites as affected by chemical composition, heating and particle size: *Clay Miner.* **13,** 241–253.

Schroeder, P. A. (1989) Phyllosilicate sample mounting for far infrared absorption spectroscopy: *Abstracts with program,* A.I.P.E.A. 9th International Clay Conference, Strasbourg, France, 343.

Schroeder, P. A. (1990) Far infrared, X-ray diffraction and chemical investigation of potassium micas: *Amer. Mineral.* **75,** 983–991.

Smith, A. L. (1965) Infrared spectroscopy: in *Treatise on Analytical Chemistry: Part 1, Theory and Practice 6,* I. M. Kothoff, P. J. Elving, and E. B. Sandell, eds., John Wiley Interscience, New York, 3535–3744.

Smith, D. K., Johnson, G. G., Jr., Scheible, A., Wims, A. M., Johnson, J. L., and Ullmann, G. (1987) Quantitative X-ray powder diffraction method using the full diffraction pattern: *Powder Diffraction* **2,** 73–77.

Środoń, J. (1980) Precise identification of illite/smectite interstratification by X-ray powder diffraction: *Clays & Clay Minerals* **28,** 401–411.

Środoń, J., Anreoli, C., Elass, F., and Robert, M. (1990) Direct high-resolution transmission electron microscopic measurement of expandability of mixed-layer illite/smectite in bentonite rock: *Clays & Clay Minerals* **38,** 373–379.

Środoń, J., Morgan, D. J., Eslinger, E. V., Eberl, D. D., and Karlinger, M. R. (1986) Chemistry of illite/smectite and end-member illite: *Clays & Clay Minerals* **34,** 368–378.

van Olphen, H. and Fripiat, J. J. (1979) *Data Handbook for Clay Minerals and other Non-metallic Minerals:* Pergamon Press, Oxford.

Velde, B. (1983) Infrared OH-stretch bands in potassic micas, talcs and saponites; influence of electron configuration and site of charge compensation: *Amer. Mineral.* **68,** 1169–1173.

Velde, B. and Couty, R. (1985) Far infrared spectra of hydrous layer silicates: *Phys. Chem. Mineral.* **12,** 347–352.

Weiss, C. A., Altaner, S. P., and Kirkpatrick, R. J. (1987) High-resolution ^{29}Si NMR spectroscopy of 2:1 layer silicates: Correlations among chemical shifts, structural distortions, and chemical variations: *Amer. Mineral.* **72,** 935–942.

Whitney, G. and Northrop, H. R. (1988) Experimental investigation of the smectite to illite reaction: Dual reaction mechanism and oxygen-isotope systematics: *Amer. Mineral.* **73,** 77–90.

Wittkop, R. and O'Day, M. (1973) Whole rock chemical analysis using the electron microprobe: *Anal. Lett.* **6,** 1021–1028.

Woessner, D. E. (1989) Characterization of clay minerals by ^{27}Al nuclear magnetic resonance spectroscopy: *Amer. Mineral.* **74,** 203–215.

(Received 23 May 1991; accepted 24 October 1991; Ms. 2106)